

Article

The Microstructural and Hardness Changes of Tungsten Fiber after Au²⁺ Irradiation

Juan Du ^{1,*}, Jialin Li ¹, Chuan Wu ², Qihang Zhang ¹, Pan Wen ², Jun Tang ², Tianyu Zhao ^{1,2,*}, Pinghuai Wang ¹, Xiang Liu ¹ and Jiming Chen ¹

¹ Southwestern Institute of Physics, Chengdu 610225, China; lij@swip.ac.cn (J.L.); zhangqihang@swip.ac.cn (Q.Z.); wangph@swip.ac.cn (P.W.); xliu@swip.ac.cn (X.L.); chenjm@swip.ac.cn (J.C.)

² Key Laboratory of Radiation Physics and Technology of Ministry of Education, Institute of Nuclear Science and Technology, Sichuan University, Chengdu 610064, China; 2021226055021@stu.scu.edu.cn (C.W.); 2020226055035@stu.scu.edu.cn (P.W.); tangjun@scu.edu.cn (J.T.)

* Correspondence: dujuan@swip.ac.cn (J.D.); zhaotianyu@swip.ac.cn (T.Z.); Tel.: +86-28-82850430 (J.D.); +86-28-82850478 (T.Z.)

Abstract: Tungsten fiber-reinforced tungsten composite (W_f/W) material is considered a plasma-facing material (PFM) with good application prospects. Commercial tungsten wire (fiber) prepared through forging and drawing processes has excellent mechanical properties, as well as a very high recrystallization temperature due to the unique texture of its grain structure. Commercial tungsten fiber is the most proper reinforcement for W_f/W. The change in the properties of tungsten fiber because of neutron irradiation makes it inevitable for W_f/W to be used as PFMs. However, there is very little research on the change in the properties of tungsten fiber caused by neutron irradiation. In this work, we used heavy ion irradiation to simulate the displacement damage generated by neutron irradiation to explore the alteration of the properties of a commercial tungsten fiber caused by neutron irradiation. The investigated subject was tungsten fiber with a diameter of 300 μm. The irradiation source was 7.5 MeV Au²⁺, which generated a maximum displacement damage of 60 dpa at a depth of 400 nm, and the irradiation influenced depth was 1000 nm. Because of the irradiation, significant lattice distortion occurred within the tungsten fiber, resulting in the transition from (110) texture to (100) texture at the fiber's cross-section. The results of the Schmidt factor and Taylor factor analysis indicate a decrease in the plasticity of the tungsten fiber after irradiation, but it did not completely lose its plasticity. The results of the nanoindentation test confirmed the radiation hardening. After irradiation, the hardness of the tungsten fiber increased by approximately 0.33 GPa, but this increase was relatively small compared to other tungsten-based materials. This indicates that commercial tungsten fiber is a low-cost and highly reliable reinforcement material for W_f/W composite materials.

Keywords: plasma-facing materials; tungsten fiber; heavy ion irradiation; irradiation hardening



Citation: Du, J.; Li, J.; Wu, C.; Zhang, Q.; Wen, P.; Tang, J.; Zhao, T.; Wang, P.; Liu, X.; Chen, J. The Microstructural and Hardness Changes of Tungsten Fiber after Au²⁺ Irradiation. *Crystals* **2023**, *13*, 920. <https://doi.org/10.3390/cryst13060920>

Academic Editor: Duc Nguyen-Manh

Received: 13 May 2023

Revised: 4 June 2023

Accepted: 5 June 2023

Published: 7 June 2023



Copyright: © 2023 by the authors. Licensee MDPI, Basel, Switzerland. This article is an open access article distributed under the terms and conditions of the Creative Commons Attribution (CC BY) license (<https://creativecommons.org/licenses/by/4.0/>).

1. Introduction

With the gradual depletion of fossil energy, human beings are in urgent need of clean, efficient and safe new sources of energy, and the development of nuclear fusion energy has attracted wide attention [1]. The magnetic confinement fusion project, International Thermonuclear Experimental Reactor (ITER), is leading the way for fusion as a future commercial energy source [2,3].

Tungsten has the advantages of a high melting point, high thermal conductivity and low sputtering rate [4], and it has been identified as a divertor material for ITER, as well as being considered one of the most promising candidate plasma-facing materials (PFMs) for future fusion reactors [5,6]. However, as a metal with a body-centered cubic (BCC) structure and because of its electronic structure, characteristics of inter atomic bonds and lattice resistance of dislocation stress field, pure tungsten materials have inherent brittleness at lower temperatures (high ductile-to-brittle transition temperature, DBTT) [7,8], brittleness

caused by recrystallization [9] and neutron irradiation when used as PFMs [10]. In the past, researchers prepared various new tungsten-based materials with significantly improved mechanical properties through doping [11], alloying [12,13] or microstructural modification methods [14]. However, in harsh service environments where high-energy neutrons, plasma and high thermal loads coexist in fusion reactors, the performance of these new materials has not been fully sufficient [15].

Long fiber-reinforced ceramic matrix composites (FCMCs) have been actively developed for high-temperature structural applications [16,17]. When a propagating primary matrix crack meets an array of fibers standing perpendicular to the crack's face, the primary crack can be deflected along the vertical interface, provided that a specific fracture's mechanical condition is satisfied. Then, the strong fibers collectively bridge the primary crack, suppressing its dynamic extension. As the applied load is increased, the interfacial debonding may continue, followed by fiber pull-out, and the matrix crack opens further in a controlled manner. The total amount of consumed energy is the measure of the apparent toughness. The toughening mechanism of an FCMC is by now well understood in terms of the fracture mechanics, where the fracture's mechanical properties at the interface are the determining parameters [18,19]. Commercial tungsten wire (from herein referred to as fiber) prepared through forging and drawing processes has extremely high deformation and significant texture [20]. The staggered connected grains and high dislocation density can increase the recrystallization temperature to over 2000 °C and maintain a strength of over 2 GPa [21]. Tungsten fiber-reinforced tungsten composite (W_f/W) material has incorporated the toughening mechanism of FCMCs by utilizing the commercial tungsten fiber as a reinforcement, which has attracted a lot of interest and achieved great success over the past years [22,23]. Mao's research [24] showed that W_f/W materials containing fine tungsten fibers can effectively improve the room temperature brittleness of tungsten and have high fracture energy.

When serving as PFMs, tungsten is expected to face severe environments, including high thermal fluxes [25], neutron irradiation [26], deuterium (D) and helium (He) plasma exposure [27,28]. The change in the properties of tungsten fiber due to neutron irradiation is inevitable for W_f/W when used as PFMs. Therefore, it is very important to understand how the reinforcement (tungsten fiber) will perform under neutron irradiation. Riesch J. [29] studied the mechanical properties of tungsten fiber after W^{6+} irradiation using tensile test investigations. The results indicate that there was a moderate decrease in strength with an increasing level of damage, while neither irradiation hardening nor reduction in ductility was detectable due to the limitation of the sample size. Apart from this, other research is scarce that reports on the degeneration of commercial tungsten fiber under displacement damage; this limits the further application of commercial tungsten fibers for use as a reinforcing phase.

In this work, we used heavy ion irradiation to simulate the displacement damage generated by neutron irradiation to explore the change in the properties of commercial tungsten fiber caused by neutron irradiation. The morphology and grain orientation of the irradiated and unirradiated samples were systematically studied via scanning transmission electron microscope (STEM) and electron back scatter diffraction (EBSD). The grain orientation parameters, such as geometrically necessary dislocations (GNDs), Schmidt factor, and Taylor factor distribution, were studied to explore the irradiation impact on the structural change in the grain. The nanoindentation test was used to analyze the irradiation hardening of the tungsten fiber. The results may provide insight into the function of the toughening mechanism for the application of W_f/W_m materials.

2. Materials and Methods

Tungsten fiber with a diameter of 300 μm (Zigong Cemented Carbide Co., Ltd., Zigong, China) was used as the subject of investigation. Heavy ion irradiation is normally used to simulate neutron irradiation for generating displacement damage on materials considering the cost and safety issues. The irradiation experiment was conducted with an HVE-3MV

Tandemron Accelerator located at Sichuan University, Key Laboratory of Radiation Physics and Technology, Ministry of Education, China. The tungsten fiber was fixed in the sample holder together with other samples to be irradiated, and the position of the tungsten fiber and the major parameters for the irradiation experiment are shown in Figure 1a. A 7.5 MeV Au^{2+} ion was utilized as the irradiation source. The samples were heated until their surfaces reached a temperature of 473 K. The heating was stopped at the beginning of the irradiation process, and the samples' surface temperatures were maintained at 376 K. The irradiation parameters are shown in the table of Figure 1, and the total accumulated fluences was 1.4×10^{16} ions cm^{-2} . The depth distribution profile of the irradiation damage was calculated using the binary collision code, Transport of Ions in Matter (TRIM, add company name, add city, add country), in the SRIM-2008 software in which the "ion distribution and quick calculation of damage" mode was chosen. The lattice binding energy (E_b) and displacement threshold energy (E_d) were set to 0 and 90 eV, respectively. The peak damage level was 60 dpa, which was calculated via Equation (1):

$$dpa = \frac{N_d \Phi}{N_w} \quad (1)$$

where N_d is the number of displacements acquired by TRIM; N_w stands for the atomic density of tungsten (6.338×10^{22} atoms cm^{-3}); and Φ stands for the ion flux, and the value is 2×10^{15} cm^{-2} h^{-1} . Figure 1b shows the depth distribution profile of the displacement damage level and the Au^{2+} concentration distribution in W. The damaged zone extends to approximately 1000 nm, and the peak damage (60 dpa) is located at approximately 400 nm. The temperature changes during the entire irradiation process were monitored using an infrared camera. Figure 1c shows the temperature distribution on the target plate at the completion of irradiation.

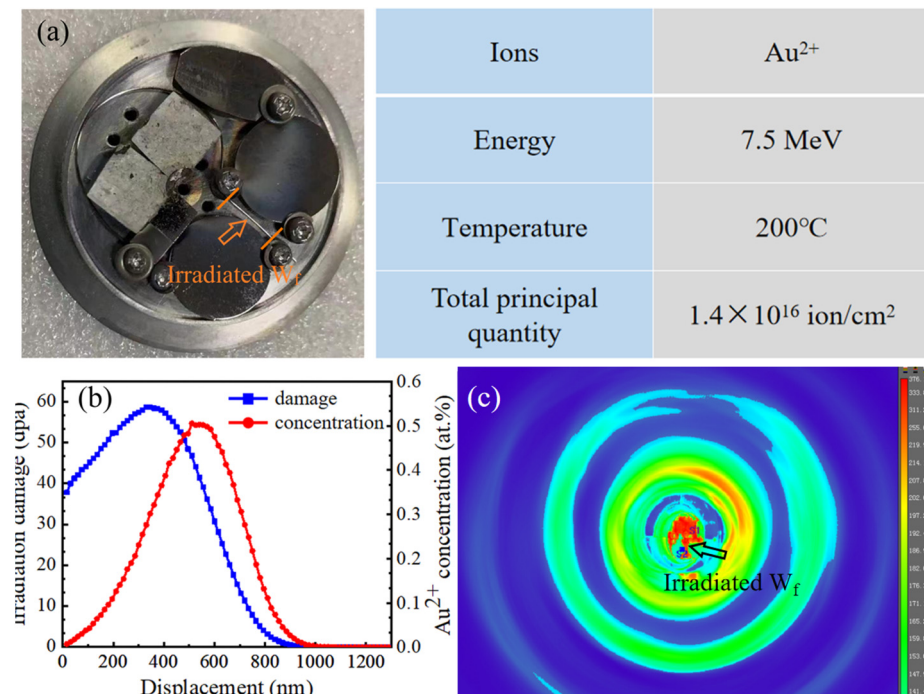


Figure 1. Au^{2+} irradiation: (a) fixation of tungsten fibers; (b) distribution profile of irradiation damage and the Au^{2+} concentration distribution; (c) temperature distribution of the target at the end of irradiation.

After the irradiation experiment, the fiber was carefully removed from the sample holder, and the irradiated side was marked. A layer of nickel metal was deposited on the outer surface to protect the structure of the fiber's outer edges during the polishing process

and to better observe the morphology of the edges during the process of microstructural analysis. The tungsten fiber with a protective nickel coating is shown in Figure 2a. Then, a short slice of the fiber was cut and embedded into the specimen holder for the polishing process. Argon ion polishing was utilized to ensure the flatness of the edges of the specimen. An image of the tungsten fiber after the polishing process is shown in Figure 2b.

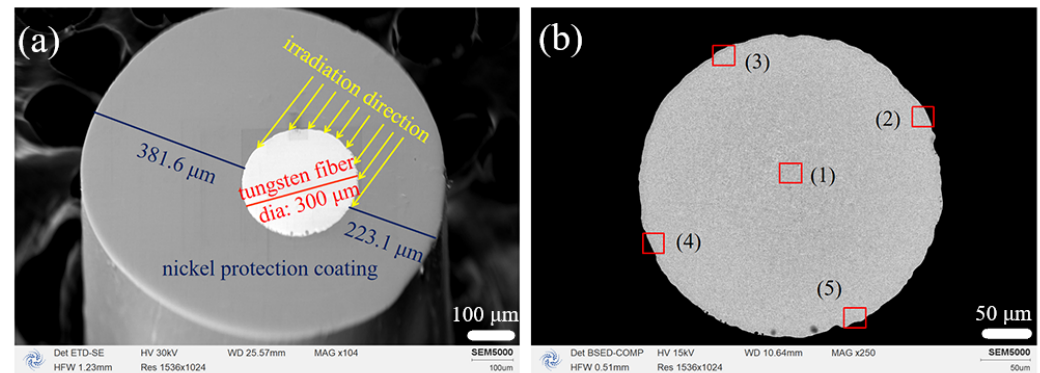


Figure 2. (a) Tungsten fiber with a protective nickel coating before the polishing process; (b) tungsten fiber after the polishing process, (1) Core of the fiber, (2) and (3) are irradiated area, (4) and (5) are un-irradiated area.

A scanning transmission electron microscope (Spectra S/TEM, NED) was used to observe the morphology of the specimens, and the electron back scatter diffraction (EBSD) technique was used to analyze the grain information of the investigated specimens. The nanohardness of the specimens was tested using a nanoindentation instrument (Keysight G200, Roseville, CA, USA).

3. Results and Discussion

As shown in Figure 2b, it can be seen that the tungsten fiber was perfectly vertically embedded into the specimen holder, and the entire cross-section was very flat. Five regions, as indicated in Figure 2b, were selected as the areas of investigation. Region 1 is located in the middle area of the tungsten fiber; regions 2 and 3 are the areas on the irradiated side and; and regions 4 and 5 are the areas that are the farthest from the irradiated side. Since the depth of the irradiation's influence was only ~ 1000 nm from the outer surface of the irradiating side, regions 1, 4 and 5 represent the unirradiated regions.

Figure 3a shows the grain morphology of region 1. This area was taken from a core of the tungsten fiber and had a good processing status. We chose this location as the reference to represent the initial state of the grain structure of the cross-section of the tungsten fiber. It can be seen that most of the grains exhibited irregular elongated shapes, and a small number of grains were an ellipsoidal shape that interlaced with each other. The distribution of the grain diameters is shown in Figure 3b, and according to the equivalent circle diameter and area weighted fraction, the average diameter of the grains is calculated to be $0.4 \mu\text{m}$. It is known that tungsten fiber is produced via multiple drawing steps, and this causes the grains to have a high deformation rate. The high grain deformation rate contributes to the fine grain size at the cross-section and interlacing [30]. Figure 3c shows the corresponding average geometrically necessary dislocation density (GND) of region 1. Because of the high deformation rate during the fiber production process, the average GND of the tungsten fiber core was as high as $28.03 \times 10^{14}/\text{m}^2$, which indicates that the fiber has great plastic deformation capability in the Z-direction. Figure 3d shows the Schmidt factor values of each grain along the $\{111\}$ packing direction $\langle 110 \rangle$. The plastic deformation of materials is mainly achieved through slip, and the higher the Schmidt factor, the greater the probability of slip system initiation. It can be seen that the Schmidt factor values of all of the grains were between 0.28 and 0.5, which indicates that the grains were in the soft orientation state and prone to slip. Figure 3e,f display the polar and inverse pole figures of the investigated

area, respectively. It can be observed that the tungsten fiber had a very strong texture $\{110\}$ due to the axial grain slip during the production (drawing) process.

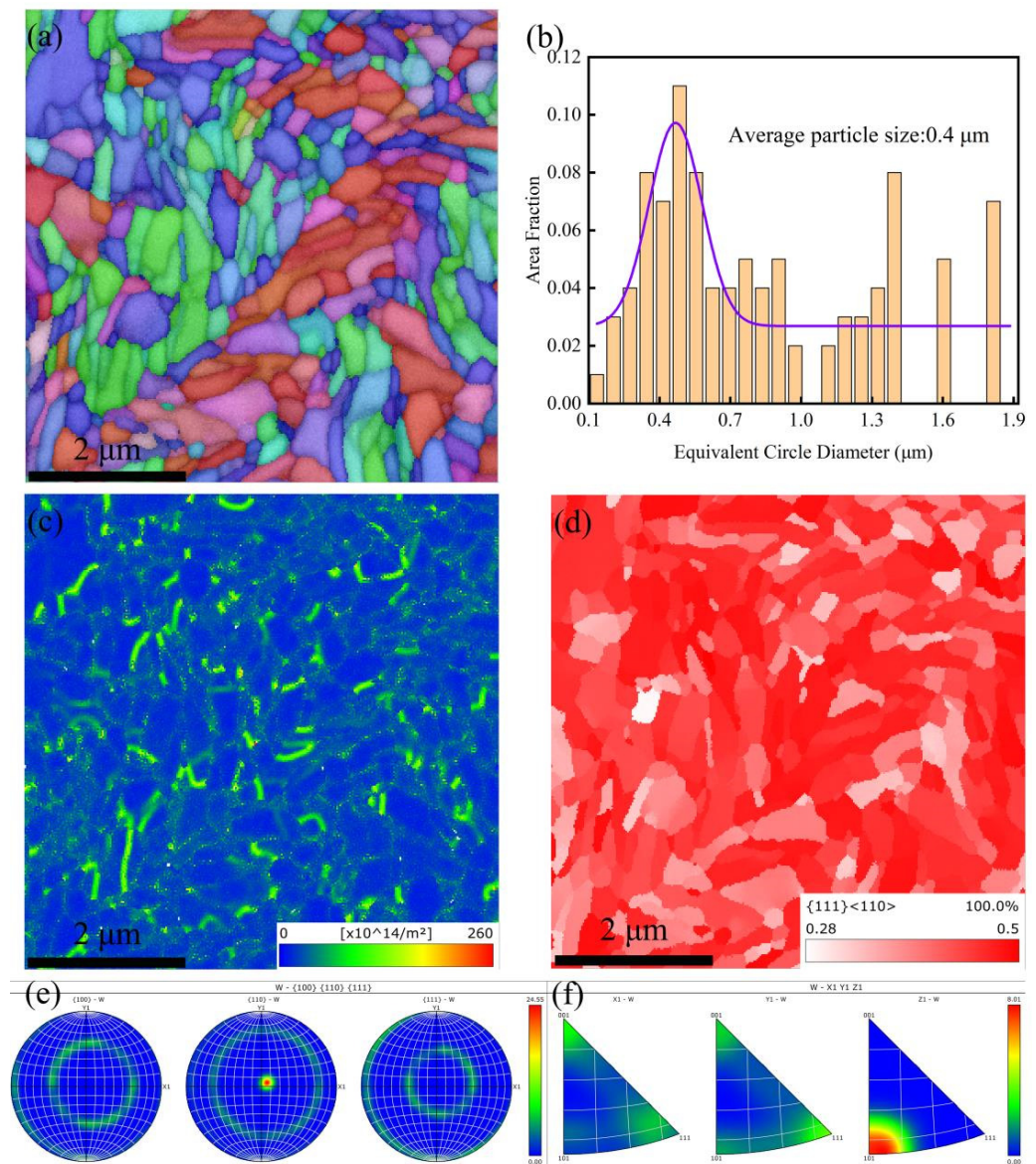


Figure 3. Microscopic morphology of region 1: (a) grain morphology and crystal orientation information; (b) distribution of the grain size of (a); (c) average geometrically necessary dislocation density (GND) statistics of (a); (d) Schmidt factor distribution of all grains in (a); (e,f) polar and inverse pole figures of the area (a), respectively.

The morphology of regions 2 and 3 are shown in Figure 4. The areas from the top edge down to 1000 nm in depth are irradiation influenced areas, while the areas at the bottom are the unirradiated areas. It can be seen that it is difficult to detect any difference in the grain structure between the irradiated and unirradiated regions. However, this does not necessarily mean that no irradiation defect was produced by the irradiation process. Therefore, a further investigation was performed to explore the impact of irradiation on the grain orientation, such as the texture of the structure of the tungsten fiber. It is known that this tungsten fiber has a texture in the grain structure, since it was produced via large deformation. High-energy ion irradiation often leads to lattice changes, and different crystal planes have different resistances to ion irradiation. For instance, a previous study showed that the (110) crystal plane of single-crystal tungsten had the best radiation

hardening resistance [31]. The irradiation influence could be detected via the change in the grain orientation.

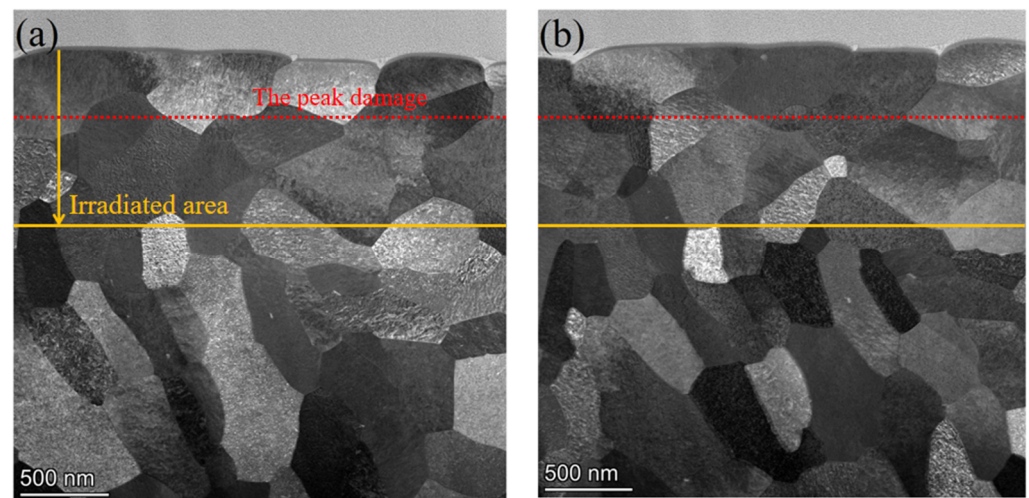


Figure 4. Microscopic morphology of tungsten fiber after irradiation: (a) STEM image of region 2; (b) STEM image of region 3.

In Figure 5, the polar and inverse pole figures of the unirradiated (regions 4 and 5) and irradiated (regions 2 and 3) regions are presented. Figure 5a,b display the information for region 4; Figure 5c,d provide the information for region 5; Figure 5e,f present the information for region 2; and Figure 5g,h show the information for region 3.

The results for the unirradiated regions (regions 4 and 5) showed a similar texture structure as region 1, which had dominant orientation in the $\{101\}$ planes when looking at the z-axis direction (see Figures 3f and 5f,h). The intensity of the dominant orientations shown in Figure 5f,h are smaller than that in Figure 3f. The reason could be that some residual stress was introduced during the drawing process at the fiber edges. The stress may have caused the distortion of the lattice and eventually a difference in the intensity of the dominant orientations [31,32].

When looking at the irradiated case (regions 2 and 3), it can be seen that their grains have multiple dominant orientations, and they mostly appeared in the $\{101\}$ and $\{001\}$ planes when looking at the z-axis direction [33]. It is interesting that the texture structures are found when looking at the x- and y-axis directions, while this phenomenon is not detected for the unirradiated case. The high-energy Au^{2+} ions were injected into the tungsten fiber through the outer surface (x- and y-axis directions) and embedded into tungsten when their energy was consumed by collision. The implanted Au atoms stayed in the tungsten material by replacing the tungsten atoms, being interstitials or by forming the second phase at the boundaries of the tungsten grains. The existing Au in the tungsten may have caused the lattice distortion for the tungsten. A distorted lattice has different lattice parameters than the original and leads to the phenomenon that the texture of the grain structure changes. This is why different dominant grain orientations were found between the irradiated and unirradiated areas.

Further comparisons of the grain structure and GND between the irradiated and un-irradiated regions are shown in Figure 6. Figure 6a shows the grain orientation in the un-irradiated area, with most of the grains appearing green at the edges, which means most grains exhibited $\{110\}$ planes. As a comparison, the grain orientation in the irradiated area is shown in Figure 6d, and more red grains can be found at the edge. This indicates that the tungsten fiber underwent significant lattice distortion during irradiation, e.g., the texture with $\{100\}$ planes was replaced with $\{110\}$ planes. Meanwhile, it can be seen that the average diameter of the grains calculated according to the equivalent circle diameter and area weighted fraction were both $0.4 \mu\text{m}$ for the irradiated and unirradiated cases

(Figure 6b,e). The average values of GND were $23.7 \times 10^{14}/\text{m}^2$ and $23.2 \times 10^{14}/\text{m}^2$ for the irradiated and unirradiated areas, respectively. The tungsten fiber still had a certain plastic deformation ability along the z-axis direction after irradiation.

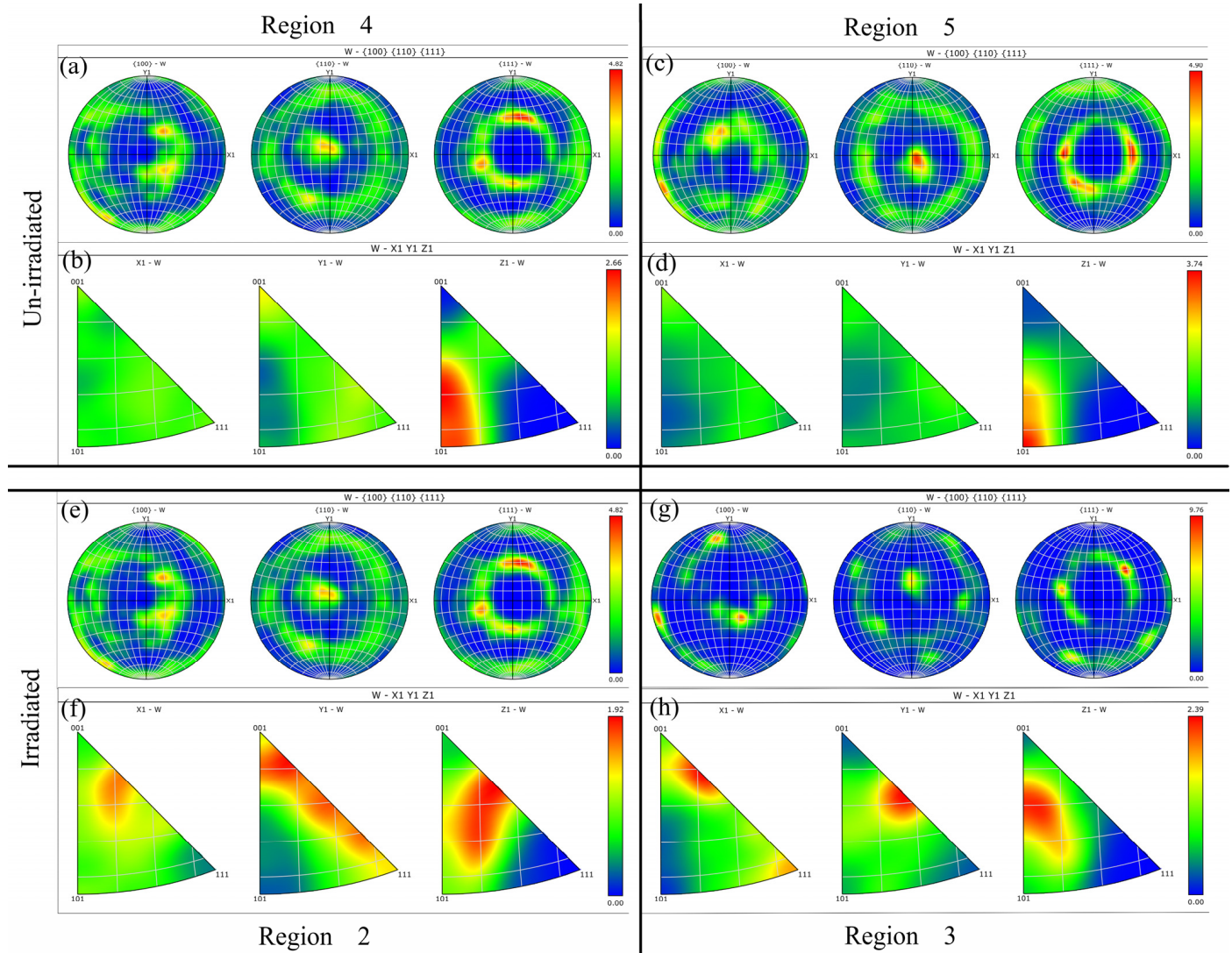


Figure 5. The polar and inverse pole figures of the irradiated and nonirradiated regions: (a,b) region 4; (c,d) region 5; (e,f) region 2; (g,h) region 3.

Figure 7 shows a comparison of the Schmidt and Taylor factors between the irradiated and unirradiated regions. For tungsten metal with a BCC lattice structure, the slip is carried out through a $\langle 111 \rangle (110)$ slip system. The higher the Schmidt factor, the greater the probability of slip system initiation. It can be seen that after irradiation, 88.7% of the grains had a Schmidt factor between 0.29 and 0.5, which is slightly lower than for the unirradiated (92.8%). The difference between the two values was only 4.1%. Considering that the irradiation influenced area was only one-sixth of the upper part of the image, the actually decrease in the Schmidt factor due to the irradiation should be higher than 4.1%.

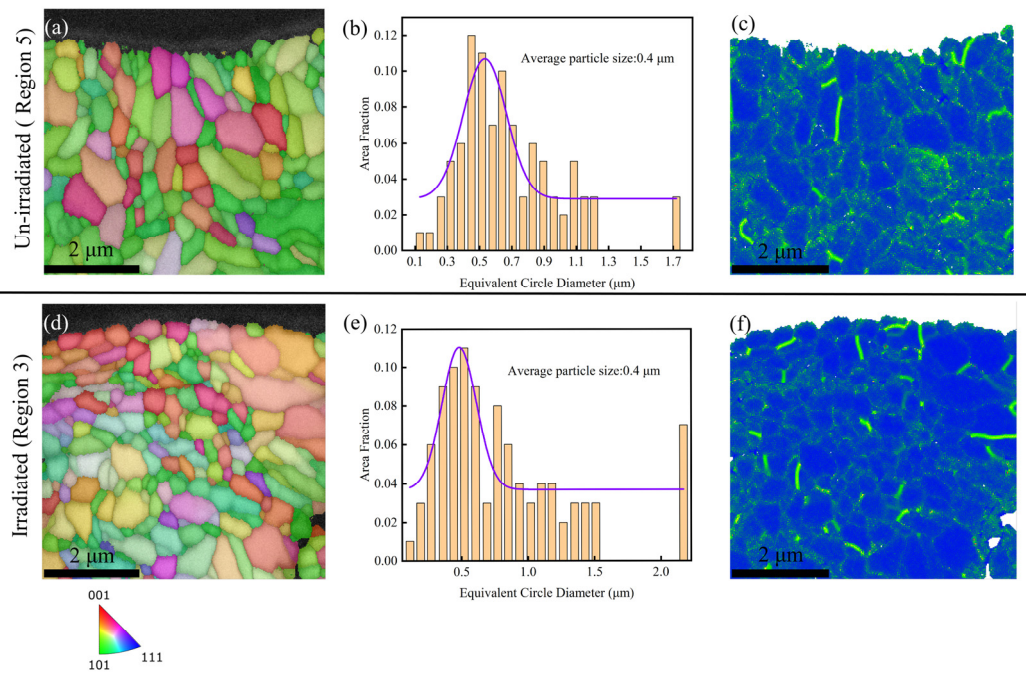


Figure 6. Microstructure of the irradiated and unirradiated regions: (a) grain boundary morphology and crystal orientation information of region 5; (b) grain size distribution in (a); (c) GND statistics in (a); (d) grain boundary morphology and crystal orientation information of region 3; (e) grain size distribution in (d); (f) GND statistics in (d).

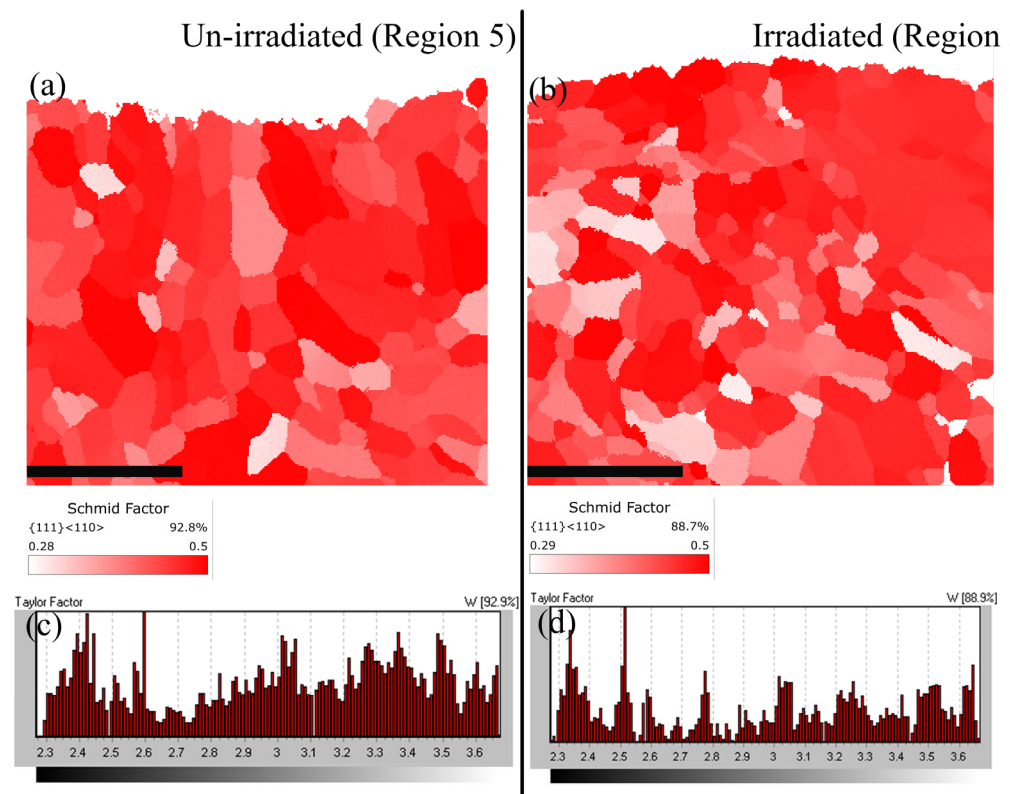


Figure 7. The Schmid factor and Taylor factor before and after irradiation: (a,b) unirradiated region; (c,d) irradiated region.

The larger the Taylor factor means the larger the plastic deformation the grain can endure under certain stress. When looking at the Taylor factor distribution result, compared

to the unirradiated areas shown in Figure 7c, the Taylor factor of the grains of the irradiated ones decreased because of the irradiation process (Figure 7d). This means the plasticity of the tungsten fiber decreased because of the irradiation defects. Nevertheless, more than half of the grains still had Taylor factor values greater than three, indicating that the tungsten fiber still had a certain degree of plasticity, which is consistent with other research results [29]. In a word, commercial tungsten fibers have the better radiation resistance compared to pure tungsten materials prepared using other processing methods.

Finally, we characterized the hardness of the irradiated and unirradiated areas using the nanoindentation test. Because of the curvature structure of the tungsten fiber’s surface, the nanoindentation test was performed in the following way: an indenter head with a diameter of 2 μm was selected for the indentation; the indentation depth was set at 400 nm, corresponding to the depth of the maximum displacement damage location. Figure 8 shows the hardness results. The average hardness of the irradiated case was 8.37 GPa, which was 0.33 GPa higher than that of the unirradiated. The degree of irradiation hardening is related to the value of displacement per atom (dpa) and the irradiation temperature. A larger dpa and higher irradiation temperature lead to greater irradiation hardening. Table 1 shows the irradiation hardening of tungsten materials prepared using different processing techniques over recent years.

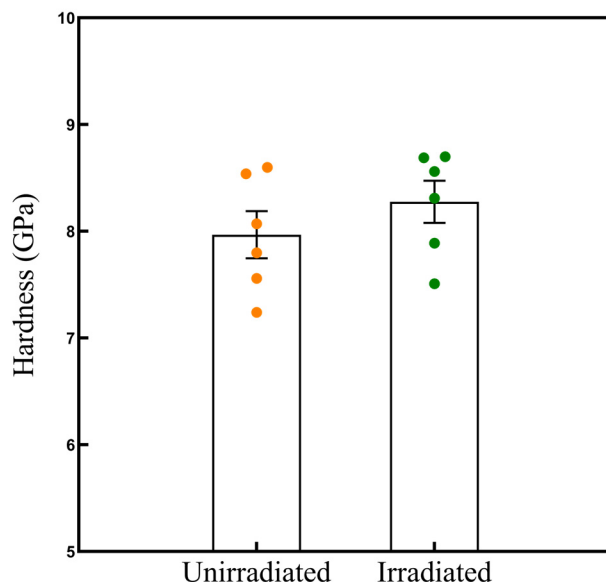


Figure 8. Changes in the hardness before and after irradiation.

Table 1. Radiation hardening of tungsten-based materials prepared using different processing methods.

Number	Materials	Processed	Irradiation Ions	Irradiation Temperature (°C)	Max Irradiation Damage (dpa)	The Depth of Maximum dpa (nm)	The Difference of Hardness (GPa)
1	KW [34]	SPS	W2+	650	11.5	400	1
2	W [35]	Rolling	W6+	500	7	110	1.1
3	KW [36]	Rolling	Fe11+	127	0.45	700	0.7
4	W-ZrO2 [37]	Swaging	Au ²⁺	RT	100	200	4.52
This work	W	Drawing	Au ²⁺	200	60	400	0.33

It can be seen that tungsten fiber (this work) had the smallest difference in the hardness (irradiation hardening) among the reported results. When compared to the reference case 3 (rolling KW), the irradiation in this work was performed at a higher irradiation temperature and large dpa, and the tungsten fiber still had a smaller irradiation hardening. It is believed that commercial tungsten fiber has good resistance to irradiation hardening

than tungsten produced via other metallurgy manufacturing processes. The good resistance to irradiation hardening may be due to the severe lattice distortion caused by the unique texture structure of the tungsten fibers as we discussed above. The severe lattice distortion in the microstructure improves the material's macroscopic resistance to radiation hardening, which is also reflected in other types of alloys [38]. This further shows that commercial tungsten fiber is a good candidate for use as a reinforcement in W_f/W composites.

4. Conclusions

- (1) Commercially, tungsten fibers with a diameter a 300 μm were irradiated with 7.5 MeV Au^{2+} . A maximum displacement damage of 60 dpa was achieved at a 400 nm depth. No clear defect was detected via STEM observation of the microstructure of the fiber cross-section.
- (2) The grains of the irradiated regions had multiple dominant orientations, and they mostly appeared in the {101} and {001} planes when looking at the z-axis direction, while the grains of the unirradiated regions had the dominant orientation in the {101} planes. The grain orientation deviation is believed to be due to the lattice distortion caused by the Au^{2+} irradiation.
- (3) The Schmidt factor of the grains slightly decreased because of the Au^{2+} irradiation, but 88.7% of the grains had a Schmidt factor between 0.29 and 0.5, which means the fiber still maintained a certain level of plastic deformation after irradiation.
- (4) The Taylor factor of the grains decreased because of the irradiation, which indicates that the plasticity of the tungsten fiber decreased because of the irradiation. More than half of the grains still had Taylor factor values greater than three, indicating that the tungsten fiber still had a certain degree of plasticity after irradiation.
- (5) The results of the nanoindentation test confirmed the radiation hardening. After irradiation, the hardness of the tungsten fibers increased by approximately 0.33 GPa, but this increase was relative compared to other tungsten-based materials. This indicates that commercial tungsten fiber is a low-cost and highly reliable reinforcing material for W_f/W composite materials.

Novelty and application: Research on commercial tungsten fiber as a reinforcing phase for W_f/W has been ongoing for several years, but due to the presence of objective factors, such as a small diameter and curved irradiation surface, it is difficult to study the microstructure and properties of irradiated fibers. In this work, we used a scanning transmission electron microscope (STEM) and the electron back scatter diffraction (EBSD) method, to investigate the influence of irradiation on the microstructure of tungsten fiber. The grain orientation parameters, such as geometrically necessary dislocations (GNDs), Schmidt factor and Taylor factor distributions, of the grains were studied to explore the irradiation impact on the grain's structural changes and then to determine the macroscopic plastic changes of the tungsten fibers, which were verified through nanoindentation tests. The results of this paper provide a theoretical basis for the application of tungsten fiber as a reinforcement for W_f/W composites, as well as for the design of W_f/W composites.

Author Contributions: Conceptualization, J.D. and T.Z.; methodology, T.Z.; validation, J.D.; formal analysis, J.L. and C.W.; investigation, Q.Z. and C.W.; resources, J.T.; data curation, C.W. and P.W. (Pan Wen); writing—original draft preparation, J.D.; writing—review and editing, P.W. (Pinghuai Wang), X.L. and J.C.; visualization, C.W.; supervision, J.C.; project administration, X.L.; funding acquisition, J.D. and X.L. All authors have read and agreed to the published version of the manuscript.

Funding: This research was funded by the National Natural Science Foundation of China (No. 12192280) and the Innovation Program of SWIP (No. 202103XWCXRC002).

Data Availability Statement: Not applicable.

Conflicts of Interest: The authors declare no conflict of interest.

References

1. Federici, G.; Bachmann, C.; Barucca, L.; Baylard, C.; Biel, W.; Boccaccini, L.V.; Bustreo, C.; Ciattaglia, S.; Cismondi, F.; Corato, V.; et al. Overview of the DEMO staged design approach in Europe. *Nucl. Fusion* **2019**, *59*, 066013. [[CrossRef](#)]
2. Litaudon, X.; Abduallev, S.; Abhangi, M.; Abreu, P.; Afzal, M.; Aggarwal, K.; Ahlgren, T.; Ahn, J.; Aho-Mantila, L.; Aiba, N.; et al. Overview of the JET results in support to ITER. *Nucl. Fusion* **2017**, *57*, 102001. [[CrossRef](#)]
3. Degraeve, J.; Felici, F.; Buchli, J.; Neunert, M.; Tracey, B.; Carpanese, F.; Ewalds, T.; Hafner, R.; Abdolmaleki, A.; de las Casas, D.; et al. Magnetic control of tokamak plasmas through deep reinforcement learning. *Nature* **2022**, *602*, 414–419. [[CrossRef](#)] [[PubMed](#)]
4. Abdou, M.; Morley, N.B.; Smolentsev, S.; Ying, A.; Malang, S.; Rowcliffe, A.; Ulrickson, M. Blanket/first wall challenges and required R&D on the pathway to DEMO. *Fusion Eng. Des.* **2015**, *100*, 2–43. [[CrossRef](#)]
5. Lifeng, T.; Pei, L.; Xuanze, L.; Yutian, M.; Xiangmin, M. Cracks and blisters formed in nanocrystalline tungsten films by helium implantation. *Fusion Eng. Des.* **2021**, *172*, 112879. [[CrossRef](#)]
6. Stork, D.; Agostini, P.; Boutard, J.; Buckthorpe, D.; Diegele, E.; Dudarev, S.; English, C.; Federici, G.; Gilbert, M.; Gonzalez, S.; et al. Developing structural, high-heat flux and plasma facing materials for a near-term DEMO fusion power plant: The EU assessment. *J. Nucl. Mater.* **2014**, *455*, 277–291. [[CrossRef](#)]
7. Lv, Y.; Hu, K.; Huang, Z.; Cao, Z.; Wen, S.; Zhao, Y.; Pan, M.; Deng, H. Effect of tungsten on vacancy behaviors in Ta-W alloys from first-principles. *Solid State Commun.* **2020**, *306*, 113767. [[CrossRef](#)]
8. Zhirkin, A.; Budaev, V.; Goltsev, A.; Dedov, A.; Komov, A.; Kuteev, B.; Lanye, I. Assessment of radiation damage of the first wall of a fusion neutron source DEMO-FNS with a blanket for the transmutation of minor actinides. *Nucl. Fusion* **2021**, *61*, 126053. [[CrossRef](#)]
9. Cui, W.; Flinders, K.; Hancock, D.; Grant, P.S. Joining and cycling performance of ultra-thick tungsten coatings on patterned steel sub-strates for fusion armour applications. *Mater. Des.* **2021**, *212*, 110250. [[CrossRef](#)]
10. Macková, A.; Fernandes, S.; Matejíček, J.; Vilémová, M.; Holý, V.; Liedke, M.O.; Martan, J.; Vronka, M.; Potoček, M.; Bátor, P.; et al. Radiation damage evolution in pure W and W-Cr-Hf alloy caused by 5 MeV Au ions in a broad range of dpa. *Nucl. Mater. Energy* **2021**, *29*, 101085. [[CrossRef](#)]
11. Lv, Y.; Han, Y.; Zhao, S.; Du, Z.; Fan, J. Nano-in-situ-composite ultrafine-grained W–Y₂O₃ materials: Microstructure, mechanical properties and high heat load performances. *J. Alloys Compd.* **2021**, *855*, 157366. [[CrossRef](#)]
12. El-Guebaly, L.A.; Setyawan, W.; Kurtz, R.J.; Odette, G.R. Neutron activation and radiation damage assessment for W-Ni-Fe tungsten heavy alloys with variable Ni content. *Nucl. Mater. Energy* **2021**, *29*, 101092. [[CrossRef](#)]
13. Wang, J.; Hatano, Y.; Hinoki, T.; Alimov, V.K.; Spitsyn, A.V.; Bobyr, N.P.; Kondo, S.; Toyama, T.; Lee, H.T.; Ueda, Y.; et al. Deuterium retention in W and binary W alloys irradiated with high energy Fe ions. *J. Nucl. Mater.* **2021**, *545*, 152749. [[CrossRef](#)]
14. Xie, X.F.; Xie, Z.M.; Liu, R.; Fang, Q.F.; Liu, C.S.; Han, W.Z.; Wu, X. Hierarchical microstructures enabled excellent low-temperature strength-ductility synergy in bulk pure tungsten. *Acta Mater.* **2022**, *228*, 117765. [[CrossRef](#)]
15. Yin, C.; Terentyev, D.; Zhang, T.; Nogami, S.; Antusch, S.; Chang, C.-C.; Petrov, R.H.; Pardo, T. Ductile to brittle transition temperature of advanced tungsten alloys for nuclear fusion applications deduced by miniaturized three-point bending tests. *Int. J. Refract. Met. Hard Mater.* **2021**, *95*, 105464. [[CrossRef](#)]
16. Deng, Y.; Li, W.; Wang, R.; Shao, J.; Geng, P.; Ma, J. The temperature-dependent fracture models for fiber-reinforced ceramic matrix composites. *Compos. Struct.* **2016**, *140*, 534–539. [[CrossRef](#)]
17. Jia, Y.; Chen, S.; Ji, X.; Gou, Y.; Li, Y.; Hu, H. High-temperature oxidation behavior and oxidation mechanism of C/SiBCN composites in static air. *Ceram. Int.* **2019**, *45*, 12764–12772. [[CrossRef](#)]
18. Lü, N.C.; Cheng, Y.H.; Li, X.G.; Cheng, J. Asymmetrical dynamic fracture model of bridging fiber pull-out of unidirectional composite materials. *Nonlinear Dyn.* **2011**, *66*, 1–14. [[CrossRef](#)]
19. Hsueh, C.-H. Interfacial debonding and fiber pull-out stresses of fiber-reinforced composites. *Mater. Sci. Eng. A* **1990**, *123*, 1–11. [[CrossRef](#)]
20. Terentyev, D.; Van Renterghem, W.; Tanure, L.; Dubinko, A.; Riesch, J.; Lebediev, S.; Khvan, T.; Verbeke, K.; Coenen, J.W.; Zhurkin, E.E. Correlation of microstructural and mechanical properties of K-doped tungsten fibers used as reinforcement of tungsten matrix for high temperature applications. *Int. J. Refract. Met. Hard Mater.* **2018**, *79*, 204–216. [[CrossRef](#)]
21. Riesch, J.; Han, Y.; Almanstötter, J.; Coenen, J.W.; Höschen, T.; Jasper, B.; Zhao, P.; Linsmeier, C.; Neu, R. Development of tungsten fibre-reinforced tungsten composites towards their use in DEMO—Potassium doped tungsten wire. *Phys. Scr.* **2016**, *2016*, 014006. [[CrossRef](#)]
22. Du, J.; You, J.-H.; Höschen, T. Thermal stability of the engineered interfaces in W_f/W composites. *J. Mater. Sci.* **2012**, *47*, 4706–4715. [[CrossRef](#)]
23. Schönen, S.; Jasper, B.; Coenen, J.W.; Du, J.; Höschen, T.; Riesch, J.; Natour, G.; Neu, R.; Linsmeier, C. Insight into single-fiber push-out test of tungsten fiber-reinforced tungsten. *Compos. Interfaces* **2018**, *26*, 107–126. [[CrossRef](#)]
24. Shu, R.; Mao, Y.; Coenen, J.W.; Terra, A.; Liu, C.; Schönen, S.; Riesch, J.; Linsmeier, C.; Broeckmann, C. Interface and mechanical properties of the single-layer long fiber reinforced W_f/W composites fabricated via field assisted sintering technology. *Mater. Sci. Eng. A* **2022**, *857*, 144098. [[CrossRef](#)]
25. Roth, J.; Tsitron, E.; Loarte, A.; Loarer, T.; Counsell, G.; Neu, R.; Philipps, V.; Brezinsek, S.; Lehnen, M.; Coad, P.; et al. Recent analysis of key plasma wall interactions issues for ITER. *J. Nucl. Mater.* **2009**, *390–391*, 1–9. [[CrossRef](#)]

26. Ueda, Y.; Coenen, J.; De Temmerman, G.; Doerner, R.; Linke, J.; Philipps, V.; Tsitrone, E. Research status and issues of tungsten plasma facing materials for ITER and beyond. *Fusion Eng. Des.* **2014**, *89*, 901–906. [[CrossRef](#)]
27. Zinkle, S.; Snead, L. Designing Radiation Resistance in Materials for Fusion Energy. *Annu. Rev. Mater. Res.* **2014**, *44*, 241–267. [[CrossRef](#)]
28. Bolt, H.; Barabash, V.; Federici, G.; Linke, J.; Loarte, A.; Roth, J.; Sato, K. Plasma facing and high heat flux materials—Needs for ITER and beyond. *J. Nucl. Mater.* **2002**, *307–311*, 43–52. [[CrossRef](#)]
29. Riesch, J.; Feichtmayer, A.; Coenen, J.; Curzadd, B.; Gietl, H.; Höschen, T.; Manhard, A.; Schwarz-Selinger, T.; Neu, R. Irradiation effects in tungsten—From surface effects to bulk mechanical properties. *Nucl. Mater. Energy* **2021**, *30*, 101093. [[CrossRef](#)]
30. Jiang, X.; Song, J.; Peng, F.; Guo, D.; Fang, Y.; Dai, S.; Zhu, B. Microstructure and High-Temperature Performance of High K-Doped Tungsten Fibers Used as Reinforcement of Tungsten Matrix. *Crystals* **2022**, *12*, 63. [[CrossRef](#)]
31. Ripoll, M.R.; Weygand, S.M.; Riedel, H. Reduction of tensile residual stresses during the drawing process of tungsten wires. *Mater. Sci. Eng. A* **2010**, *527*, 3064–3072. [[CrossRef](#)]
32. Ripoll, M.R.; Oenák, J. Microstructure and texture evolution during the drawing of tungsten wires. *Eng. Fract. Mech.* **2009**, *76*, 1485–1499. [[CrossRef](#)]
33. Hasenhuettl, E.; Zhang, Z.; Yabuuchi, K.; Kimura, A. Effect of displacement damage level on the ion-irradiation affected zone evolution in W single crystals. *J. Nucl. Mater.* **2017**, *495*, 314–321. [[CrossRef](#)]
34. Qiu, W.B.; Chen, L.Q.; Yang, X.L.; Deng, H.; Liu, C.S.; Zhang, K.; Tang, J. Hardening effect of multi-energy W²⁺-ion irradiation on tungsten–potassium alloy. *Chin. Phys. B* **2020**, *29*, 421–427.
35. Yu, J.; Kurotaki, H.; Ando, M.; Nozawa, T. Mechanical properties of self-ion irradiated pure tungsten using nano-indentation test and micro-tensile test. *Nucl. Mater. Energy* **2022**, *30*, 101145. [[CrossRef](#)]
36. Ma, X.; Zhang, X.; Wang, T.; Lv, W.; Lang, S.; Ge, C.; Yan, Q. Irradiation hardening behaviors of large-scale hot rolling potassium-doped tungsten alloy under synergistic irradiations of Fe 11+ ion combined with deuterium and helium plasmas. *Nucl. Mater. Energy* **2022**, *30*, 101138. [[CrossRef](#)]
37. Cui, B.; Luo, C.; Chen, X.; Zou, C.; Li, M.; Xu, L.; Yang, J.; Meng, X.; Zhang, H.; Zhou, X.; et al. Superior Radiation Resistance of ZrO₂-Modified W Composites. *Materials* **2022**, *15*, 1985. [[CrossRef](#)]
38. Chen, Y.; Wang, S.; Feng, H.; Li, W.; Liu, B.; Li, J.; Liu, Y.; Liaw, P.K.; Fang, Q. Irradiation hardening behavior of high entropy alloys using random field theory informed discrete dislocation dynamics simulation. *Int. J. Plast.* **2023**, *162*, 103497. [[CrossRef](#)]

Disclaimer/Publisher’s Note: The statements, opinions and data contained in all publications are solely those of the individual author(s) and contributor(s) and not of MDPI and/or the editor(s). MDPI and/or the editor(s) disclaim responsibility for any injury to people or property resulting from any ideas, methods, instructions or products referred to in the content.